Journal of Organometallic Chemistry 696 (2011) 3882–3894

Contents lists available at SciVerse ScienceDirect

Journal of Organometallic Chemistry

journal homepage: www.elsevier.com/locate/jorganchem

Synthesis and electrochemistry of 1,1′-bis(phosphino)cobaltocenium compounds

Kyle D. Reichl[a,1], Chelsea L. Mandell[a], Owen D. Henn[a,2], William G. Dougherty[b], W. Scott Kassel[b], Chip Nataro[a,*]

[a] Department of Chemistry, Lafayette College, Easton, PA 18042, USA
[b] Department of Chemistry, Villanova University, Villanova, PA 19085, USA

ARTICLE INFO

Article history:
Received 18 August 2011
Received in revised form
30 August 2011
Accepted 2 September 2011

Keywords:
Electrochemistry
Cyclic voltammetry
Crystal structures
Cobaltocenium
Phosphine

ABSTRACT

The electrochemistry of 1,1′-bis(diphenylphosphino)cobaltocenium hexafluorophosphate ([dppc][PF_6]), 1,1′-bis(dicyclohexylphosphino)cobaltocenium hexafluorophosphate ([dcpc][PF_6]), 1,1′-bis(di-iso-propylphosphino)cobaltocenium hexafluorophosphate ([dippc][PF_6]), and 1-(di-tert-butylphosphino)cobaltocenium hexafluorophosphate ([1-dtbpc][PF_6]) was examined in methylene chloride with tetrabutylammonium hexafluorophosphate as the supporting electrolyte. A reversible reductive wave followed by an irreversible wave at more negative potentials was observed. Ten new phosphinothioyl ([dppcS_2][PF_6], [dcpcS_2][PF_6], [dippcS_2][PF_6], [1-dtbpcS][PF_6], and 1,1′-bis(dicyclohexylphosphinothioyl)ferrocene) and phosphinoselenoyl derivatives ([dppcSe_2][PF_6], [dcpcSe_2][PF_6], [dippcSe_2][PF_6], [1-dtbpcSe][PF_6], and 1,1′-bis(dicyclohexylphosphinoselenoyl)ferrocene) were prepared and characterized, and the structures of eight of these compounds were determined. The electrochemistry of these phosphinochalcogenyl cobaltocenium compounds, as well as the previously prepared [dppcO_2][PF_6], displayed two reversible reductive waves at potentials less negative than that of the free phosphines. A correlation was found to exist between the Hammett substituent constant σ_p and the reduction potentials of these compounds. In addition, the phosphinoselenoyl [dppcSe_2][PF_6], [dcpcSe_2][PF_6], and [dippcSe_2][PF_6] displayed an electrochemically irreversible oxidative wave, potentially indicating an intramolecular Se–Se bonded trication. The electrochemistry of three new and five previously reported transition metal complexes of the general formula [M_nCl_2($P^{\cap}P$)][PF_6] (M = Pd or Pt, n = 1, $P^{\cap}P$ = dppc, dcpc or dippc; M = Au, n = 2, $P^{\cap}P$ = dppc or dcpc)) was also examined displaying at least two reductive waves at potentials less negative than that of the free phosphines. Comparison of the electrochemical data with that previously obtained for analogous ferrocenes indicates that a correlation exists between the reduction potentials of the cobaltocenium phosphines and the potentials at which oxidation of the ferrocene phosphines occurs. In addition, the structure of [Au_2Cl_2(dppc)][PF_6] was determined.

1. Introduction

Bis(phosphino)metallocene ligands are of particular interest in catalytic applications due to their relatively high rates of electron transfer and unique stereochemical properties [1–7]. Undoubtedly the most recognized and researched ligand of this type is 1,1′-bis(diphenylphosphino)ferrocene (dppf) which has been successfully employed in various catalytic reactions such as the palladium-catalyzed Suzuki, Heck, and Buchwald-Hartwig coupling reactions [2–8]. Despite the success of these catalytic systems, the homogeneous nature of these catalysts has several drawbacks including difficulty in the isolation of the desired product, recovery and recycling of the catalyst, and the requirement of organic solvents [9]. A variety of options have been considered to limit or eliminate such drawbacks such as supporting Pd-catalysts on a polymer [10] and using ionic liquids as solvents [9]. Coupled with their low volatility and ability to readily dissolve transition metal complexes, ionic liquids provide an excellent “green” option to sequester and recycle valuable catalysts within a single liquid phase [11].

Recently, there have been several reports within the literature successfully utilizing 1,1′-bis(diphenylphosphino)cobaltocenium cation (dppc$^+$), the isoelectronic analogue of dppf, as a ligand for transition metal catalyzed reactions in ionic liquids. Ren has shown that the catalytic system [$PdCl_2$(dppc)][PF_6]/[BMIM][PF_6] (BMIM = 1-butyl-3-methyl imidazolium) was active in the Suzuki

* Corresponding author. Tel.: +1 610 330 5216; fax: +1 610 330 5714.
E-mail address: nataroc@lafayette.edu (C. Nataro).
[1] Present address: Department of Chemistry, Pennsylvania State University, University Park, PA 16802.
[2] Present address: Church & Dwight Co., Inc., Princeton, NJ 08543.

0022-328X/$ – see front matter © 2011 Elsevier B.V. All rights reserved.
doi:10.1016/j.jorganchem.2011.09.004

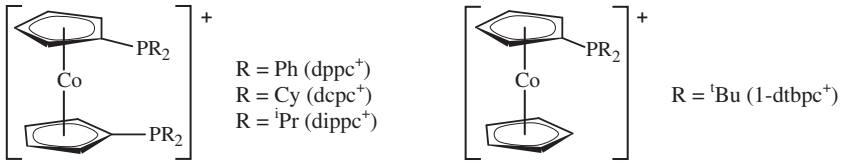

Fig. 1. Phosphinocobaltocenium cations.

coupling reaction between several aryl bromides and phenylboronic acid giving the products in excellent yields [9]. The same system was also applied to the Sonogashira coupling reaction between aryl iodides and several aryl- and alkyl-acetylenes with exceptional results [12]. In addition, dppc$^+$ was utilized in the biphasic rhodium-catalyzed hydroformylation of 1-octene in [BMIM][PF_6], giving high selectivity of *n*-nonanal [13]. In each instance, no apparent leaching of the metal catalyst into the organic phase was observed, and the catalytic solution was recovered and recycled with minimal loss of activity. The [$PdCl_2$(dppc)]][PF_6]/[BMIM][PF_6] catalytic system did not exhibit significant loss of activity in the Suzuki reaction after 140 uses, which was attributed to tight complexation of the catalyst with the ionic liquid [9,12]. Repeating the Suzuki and hydroformylation reactions with the analogous dppf catalyst resulted in significant leaching of the catalyst into the organic phase, in addition to reduced activity of the catalytic solution. Similar loss of catalytic activity was also observed upon repeating the Sonogashira reaction with [$PdCl_2(PPh_3)_2$]/[BMIM][PF_6] [14].

With such significant differences, it is surprising that relative to dppf, little research into the properties of dppc$^+$ and its derivatives has been undertaken. Many of the reported studies of dppc$^+$ and the 19-electron 1,1′-bis(diphenylphosphino)cobaltocene (dppc) involve the ligand bound to molybdenum, ruthenium, and rhenium carbonyl complexes and have examined the electrochemistry of these compounds [1,15–17]. Free dppc$^+$ displays two reductive waves, the less negative of which is reversible [1]. Complexation of dppc$^+$ generally increased the reversibility of the second reductive wave which was attributed to the bidentate coordination of the ligand [1,16,17]. The electrochemical and catalytic studies, in addition to the reduced reactivity of the cyclopentadienyl rings imparted by the central cobalt atom [13], suggest that dppc$^+$ and its derivatives are potentially useful ligands for transition metal catalysis in ionic liquids. These ligands also provide a unique opportunity to study the reactivity and electrochemical properties of charged, stable bis(phosphino)metallocenes, and compare these results to the well-characterized, netural ferrocene analogues.

Since the effect of varying phosphine substituent effects has not been investigated for derivatives of dppc$^+$, the electrochemistry of 1,1′-bis(dicyclohexylphosphino)cobaltocenium (dcpc$^+$) and 1,1′-bis(di-iso-propylphosphino)cobaltocenium (dippc$^+$) cations was performed (Fig. 1). Phosphinothioyls and phosphinoselenoyls, as well as transition metal complexes of each ligand were synthesized and characterized by NMR spectroscopy and electrochemistry. For comparison, the previously unreported phosphinothioyl and phosphinoselenoyl of 1,1′-bis(dicyclohexylphosphino)ferrocene were prepared and characterized. The electrochemistry of the monophosphine 1-(di-tert-butylphosphino)cobaltocenium cation (1-dtbpc$^+$), as well as the phosphinothioyl and phosphinoselenoyl, was also analyzed. X-ray structures of eight of the phosphinothioyls and phosphinoselenoyls as well as that of [Au_2Cl_2(dppc)][PF_6] are also reported. In addition, a new preparation of the previously synthesized phosphine oxide [dppcO_2][PF_6] [18] is also described.

Table 1
Crystal data and structure refinement for phosphinothioyl X-ray structures.

	[dcpcS_2][PF_6]	dcpfS_2	[dppcS_2][PF_6]	[1-dtbpcS][PF_6]
Formula	$C_{36}H_{56}Cl_4CoF_6P_3S_2$	$C_{34}H_{52}FeP_2S_2$	$C_{17}H_{14}Co_{0.50}F_3P_{1.50}S$	$C_{18}H_{27}CoF_6P_2S$
FW	960.57	642.67	383.26	510.33
Crystal system	Triclinic	Monoclinic	Monoclinic	Orthorohombic
Space Group	$P\bar{1}$	$P2_1/c$	C2/c	Pbca
a (Å)	12.7138(3)	11.5769(11)	30.8091(10)	7.6368(8)
b (Å)	13.3874(4)	29.015(3)	6.8241(2)	15.2489(19)
c (Å)	15.2744(4)	10.3153(9)	17.5448(7)	36.500(5)
α (Å)	83.588(1)	90	90	90
β (Å)	66.646(1)	106.322(3)	118.188(3)	90
γ (Å)	65.582(1)	90	90	90
V (Å^3)	2169.06(10)	3325.3(6)	3251.22(19)	4250.5(9)
Z	2	4	8	8
D_{calc}	1.471	1.284	1.566	1.595
Crystal size	0.14 × 0.11 × 0.11	0.19 × 0.16 × 0.10	0.18 × 0.12 × 0.02	0.16 × 0.15 × 0.12
Crystal color	Yellow	Orange	Yellow	Yellow
Temperature (K)	100(2)	100(2)	100(2)	135(2)
Absorption coefficient	0.901	0.697	0.864	1.109
F(000)	996	1376	1560	2096
θ Range (°)	2.80–33.47	1.96–33.18	2.34–33.20	2.23–33.31
Data collected				
h	−19 to 19	−17 to 17	−47 to 46	−11 to 10
k	−20 to 20	−44 to 29	−9 to 10	−14 to 23
l	−23 to 21	−15 to 15	−27 to 26	−40 to 56
Absorption correction	SADABS	SADABS	SADABS	SADABS
R, *wR* [I > $^2\sigma$(I)][a]	0.0396, 0.0870	0.0321, 0.0727	0.0406, 0.0750	0.0482, 0.1025
R, *wR* (all data)[a]	0.0625, 0.0958	0.0469, 0.0787	0.0826, 0.0873	0.0927, 0.1187
Goodness-of-fit on F^2	1.023	1.017	1.003	1.006

[a] Quantity minimized $= R(wF^2) = \sum[w(F_0^2 - F_c^2)^2]/\sum[(wF_0^2)^2]^{0.5}$; $R = \Sigma\Delta/\Sigma(F_0)$, $\Delta = |(F_0 - F_c)|$, $w = 1/[\sigma^2(F_0^2) + (aP)^2 + bP]$, $P = [2F_c^2 + \mathrm{Max}(F_0, 0)]/3$

Table 2
Crystal data and structure refinement for phosphinoselenoyl X-ray structures.

	[dcpcSe$_2$][PF$_6$]	dcpfSe$_2$	[dppcSe$_2$][PF$_6$]	[1-dtbpcSe][PF$_6$]
Formula	$C_{52.50}H_{81}Cl_{2.50}Co_{1.50}F_9P_{4.50}Se_3$	$C_{34}H_{52}FeP_2Se_2$	$C_{52.50}H_{81}Cl_{2.50}Co_{1.50}F_9P_{4.50}Se_3$	$C_{18}H_{27}CoF_6P_2Se$
FW	1436.44	736.47	860.32	557.23
Crystal system	Monoclinic	Triclinic	Monoclinic	Monoclinic
Space Group	P2/n	$P\bar{1}$	$P2_1/c$	$P2_1/c$
a (Å)	25.9240(6)	11.3523(11)	17.968(5)	19.165(3)
b (Å)	9.6293(2)	12.3513(12)	10.509(3)	7.8356(11)
c (Å)	26.4985(6)	13.6862(17)	18.884(5)	15.012(2)
α (Å)	90	97.085(5)	90	90
β (Å)	115.822(1)	110.003(5)	116.100(6)	106.141(5)
γ (Å)	90	104.593(6)	90	90
V (Å^3)	5954.3(2)	1698.1(3)	3202.0(14)	2165.6(5)
Z	4	2	4	4
D_{calc}	1.602	1.440	1.785	1.709
Crystal size	0.14 × 0.13 × 0.05	0.18 × 0.10 × 0.05	0.20 × 0.16 × 0.10	0.17 × 0.11 × 0.04
Crystal color	Orange	Orange	Orange	Yellow
Temperature (K)	100(2)	100(2)	110(2)	150(2)
Absorption coefficient	6.337	2.703	3.020	2.673
F(000)	2918	760	1704	1120
θ Range (°)	1.71–33.25	3.01–33.31	2.28–33.82	2.73–33.19
Data collected				
h	−39 to 37	−17 to 17	−27 to 27	−29 to 28
k	−14 to 10	−19 to 19	−14 to 16	−12 to 12
l	−40 to 40	−11 to 20	−29 to 25	−18 to 23
Absorption correction	SADABS	SADABS	SADABS	SADABS
R, *wR* [I > $^2\sigma$(I)][a]	0.0457, 0.0783	0.0605, 0.1100	0.0427, 0.1170	0.0414, 0.0787
R, *wR* (all data)[a]	0.0872, 0.0860	0.1691, 0.1387	0.0666, 0.1290	0.0840, 0.0906
Goodness-of-fit on F^2	1.011	1.018	1.028	1.005

[a] Quantity minimized $= R(wF^2) = \sum[w(F_0^2 - F_c^2)^2]/\sum[(wF_0^2)^2]^{0.5}$; $R = \Sigma\Delta/\Sigma(F_0)$, $\Delta = |(F_0 - F_c)|$, $w = 1/[\sigma^2(F_0^2) + (aP)^2 + bP]$, $P = [2F_c^2 + \mathrm{Max}(F_0, 0)]/3$

2. Experimental

2.1. General procedures

All reactions were carried out under an argon atmosphere using standard Schlenk techniques. Dicyclopentadiene, $ClPPh_2$, ClP^tBu_2, *n*-BuLi (1.6 M in hexanes), C_2Cl_6, ammonium hexafluorophosphate, [$PdCl_2(CH_3CN)_2$], [$PtCl_2(CH_3CN)_2$], and hydrogen peroxide were purchased from Aldrich Chemical Co., Inc. Selenium, H[$AuCl_4$]•H_2O, $ClPCy_2$, ClP^iPr_2, and dcpf were purchased from Strem Chemicals, Inc. All reagents were used without further purification. Ferrocene was purchased from Strem Chemicals, Inc. and sublimed prior to use. $CoCl_2$•$6H_2O$ and tetrabutylammonium hexafluorophosphate ([NBu_4][PF_6]) were purchased from Aldrich Chemical Co. and dried at 100 °C under vacuum. Methylene chloride (CH_2Cl_2), diethyl ether (Et_2O), hexanes, and THF were purified under argon using a Solv-tek purification system [19]. Chloroform ($CHCl_3$), water, nitromethane, 1,2-dichloroethane, di-iso-propyl ether and methanol were degassed prior to use. Dimethylformamide (DMF) was purified according to literature procedure [20]. All column chromatography was performed using silica gel as the stationary phase. The compounds [dppc][PF_6] [13], [dcpc][PF_6] [21], [dippc][PF_6] [21], [1-dtbpc][PF_6] [21], [Au_2Cl_2(dppc)][PF_6] [22], [Au_2Cl_2(dcpc)][PF_6] [22], and [$PtCl_2$(dppc)][PF_6] [23] were synthesized according to the literature procedures. ^{1}H and ^{31}P{^{1}H} NMR spectra were obtained in $CDCl_3$ unless otherwise noted, using a JEOL Eclipse 400 FT-NMR spectrometer. The ^{31}P{^{1}H} spectra were referenced to an external sample of 85% H_3PO_4, and the ^{1}H spectra were referenced to an internal TMS standard.

2.2. Preparation of [dppcO$_2$][PF$_6$]

[dppc][PF_6] (0.1406 g, 0.200 mmol) was dissolved in THF (70 mL) and cooled to 0 °C. Chilled H_2O_2 (48.1 μL, 0.471 mmol, 30 wt.% in H_2O) was added, and the solution was allowed to stir at ambient temperature for 1.5 h. After removing the solvent *in vacuo*, the resulting yellow residue was dissolved in CH_2Cl_2 (5 mL), dried over Na_2SO_4, and filtered via cannula. The solvent was removed *in vacuo*, and the resulting residue was washed with Et_2O (3 × 3 mL) and dried *in vacuo* to yield 0.1278 g (87% yield) of [dppcO$_2$][PF_6] as a yellow solid. ^{31}P NMR: δ (ppm) 20.7 (s), −143.8 (sept, $^1J_{P\text{-}F} = 711$ Hz).

Table 3
Crystal data and structure refinement for phosphinothioyl X-ray structures.

	[Au_2Cl_2(dppc)][PF_6]
Formula	$C_{42}H_{44}Au_2Cl_{10}CoF_6P_3$
FW	1563.05
Crystal system	Monoclinic
Space Group	$P2_1/n$
a (Å)	17.8836(8)
b (Å)	13.1421(6)
c (Å)	20.4629(9)
α (Å)	90
β (Å)	104.6250(10)
γ (Å)	90
V (Å^3)	4653.5(4)
Z	4
D_{calc}	2.231
Crystal size	0.16 × 0.12 × 0.03
Crystal color	Yellow
Temperature (K)	100(2)
Absorption coefficient	7.378
F(000)	3000
θ Range (°)	1.35–33.13
Data collected	
h	−24 to 27
k	−19 to 20
l	−31 to 25
Absorption correction	SADABS
R, *wR* [I > $^2\sigma$(I)][a]	0.0316, 0.0576
R, *wR* (all data)[a]	0.0528, 0.0611
Goodness-of-fit on F^2	1.023

[a] Quantity minimized $= R(wF^2) = \sum[w(F_0^2 - F_c^2)^2]/\sum[(wF_0^2)^2]^{0.5}$; $R = \Sigma\Delta/\Sigma(F_0)$, $\Delta = |(F_0 - F_c)|$, $w = 1/[\sigma^2(F_0^2) + (aP)^2 + bP]$, $P = [2F_c^2 + \mathrm{Max}(F_0, 0)]/3$

Table 4
Comparison of the redox potentials and Hammett parameters (σ_p) for ferrocene and cobaltocenium derivatives. Potentials (V vs. $FcH^{0/+}$) were measured in CH_2Cl_2 with $[NBu_4][PF_6]$ as the supporting electrolyte.

Substituent (X)	$Fe(C_5H_4X)_2$				$[Co(C_5H_4X)_{2-n}(C_5H_5)_n][PF_6]$			
	σ_p	Reference	E^0	Reference	n	E^0	E_p^{red}	Reference
–H	0.00	[25]	0.00	[26]	0	–1.33		[20]
$-PPh_2$	0.19	[25]	0.24	[27]	0	–1.14	–2.32	this work
$-PCy_2$	–0.04	[28]	0.02	[28]	0	–1.27	–2.42	this work
$-P^iPr_2$	0.06	[25]	0.05	[29]	0	–1.25	–2.37	this work
$-P^tBu_2$	0.15	[25]	0.06	[30]	1	–1.27		this work

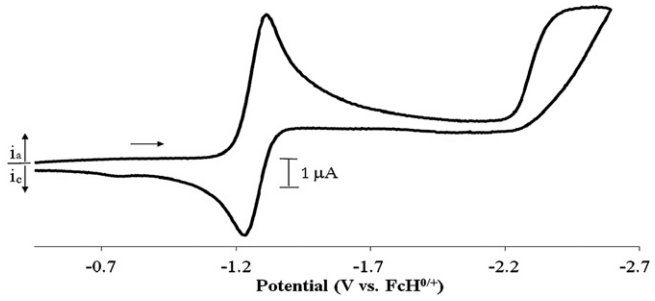

Fig. 2. CV scan for the reduction of 1.0 mM [dcpc][PF_6] in CH_2Cl_2 with 0.1 M $[NBu_4][PF_6]$ as the supporting electrolyte at 100 mV/s.

^{1}H NMR: δ (ppm) 7.62 (m, 20H, C_6H_5), 5.96 (s, 4H, C_5H_4), 5.74 (s, 4 H, C_5H_4). Anal. Calcd for $C_{34}H_{28}CoF_6O_2P_3$0.25 CH_2Cl_2: C, 54.44; H, 3.80. Found: C, 54.23; H, 3.63.

2.3. Preparation of phosphinothioyls

2.3.1. [dppcS$_2$][PF$_6$]

A solution of [dppc][PF_6] (0.0999 g, 0.142 mmol) and sulfur (0.0094 g, 0.29 mmol) in CH_2Cl_2 (20 mL) was refluxed for 5 days. Removal of solvent *in vacuo*, followed by column chromatography using CH_2Cl_2 as the eluent, yielded 0.0283 g (26% yield) of [dppcS$_2$][PF_6] as a yellow solid upon removal of the solvent. ^{31}P NMR: δ (ppm) 34.5 (s), –143.9 (sept, $^1J_{P\text{-}F} = 711$ Hz). ^{1}H NMR: δ (ppm) 7.64 (m, 20H, C_6H_5), 5.99 (s, 4H, C_5H_4), 5.64 (s, 4 H, C_5H_4). Anal. Calcd for $C_{34}H_{28}CoF_6P_3S_2$0.25 CH_2Cl_2: C, 52.22; H, 3.65. Found: C, 51.94; H, 3.58.

2.3.2. [dcpcS$_2$][PF$_6$]

A solution of [dcpc][PF_6] (0.0991 g, 0.136 mmol) and sulfur (0.0097 g, 0.302 mmol) in CH_2Cl_2 (20 mL) was refluxed overnight. Upon cooling to room temperature the solution was filtered, and the volume of solvent was reduced to approximately 5 mL *in vacuo*. The addition of Et_2O resulted in the formation of a yellow precipitate. The solution was filtered via cannula. The resulting yellow solid was washed with Et_2O (3 × 5 mL), and dried *in vacuo* to yield 0.0882 g (82% yield) of [dcpcS$_2$][PF_6]. ^{31}P NMR: δ (ppm) 53.9 (s), –143.7 (sept, $^1J_{P\text{-}F} = 711$ Hz). ^{1}H NMR: δ (ppm) 6.12 (s, 4H, C_5H_4), 5.96 (s, 4 H, C_5H_4), 2.20–1.12 (m, 44H, C_6H_{11}). Anal. Calcd for $C_{34}H_{52}CoF_6P_3S_2$: C, 51.64; H, 6.63. Found: C, 51.33; H, 6.62.

2.3.3. dcpfS$_2$

A solution of dcpf (0.1579 g, 0.273 mmol) and sulfur (0.0179 g, 0.558 mmol) in 25 mL of chloroform was refluxed for 2 h. Upon cooling the solution was filtered via cannula and the filtrate was dried *in vacuo*. Column chromatography using 2:1 (v/v) hexanes: CH_2Cl_2 as the eluent yielded 0.0754 g (43% yield) of pure dcpfS$_2$ as an orange solid upon removal of the solvent. ^{31}P NMR: δ (ppm) 57.3 (s). ^{1}H NMR: δ (ppm) 4.74 (br s, 4H, –C_5H_4) 4.42 (br s, 4H, C_5H_4) 1.32 (m, 44H, C_6H_{11}). Anal. Calcd for $C_{34}H_{52}FeP_2S_2C_6H_{14}$: C, 65.91; H, 9.13. Found: C, 66.13; H, 9.11.

2.3.4. [dippcS$_2$][PF$_6$]

A solution of [dippc][PF_6] (0.0248 g, 0.0438 mmol) and sulfur (0.0029 g, 0.090 mmol) in CH_2Cl_2 (15 mL) was refluxed overnight. Upon cooling the solution was filtered, and the volume of solvent was reduced to approximately 5 mL *in vacuo*. The addition of Et_2O

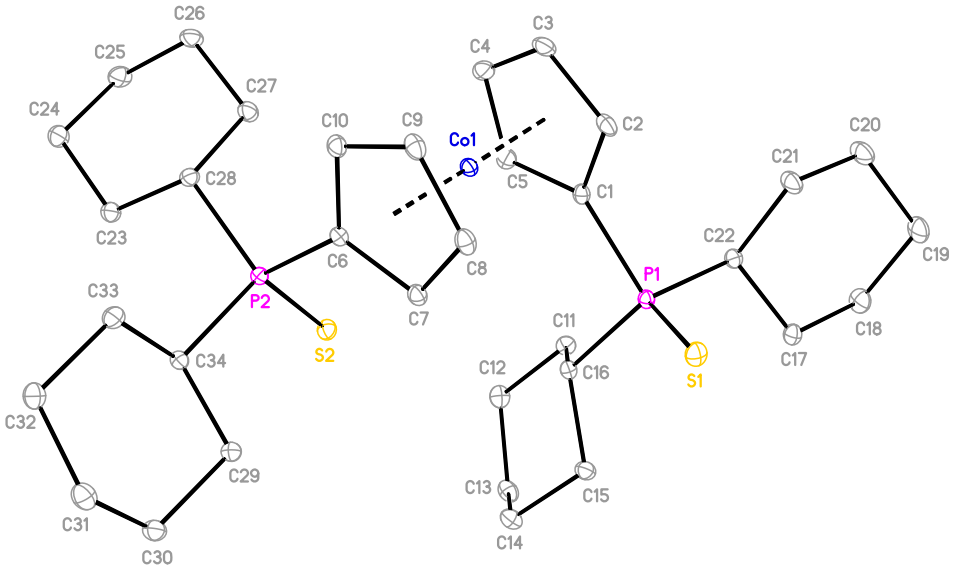

Fig. 3. Perspective view of [dcpcS$_2$][PF_6] with 30% ellipsoids. H atoms and PF_6^- omitted for clarity.

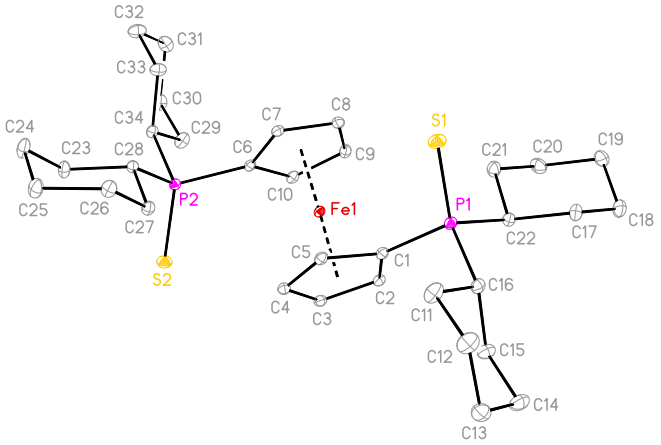

Fig. 4. Perspective view of dcpfS$_2$ with 30% ellipsoids. H atoms omitted for clarity.

resulted in the formation of a yellow precipitate. The solution was filtered via cannula, and the filtrate was washed with Et_2O (3 × 5 mL), and dried *in vacuo* to yield 0.0246 g (89% yield) of yellow [dippcS$_2$][PF$_6$]. ^{31}P NMR: δ (ppm) 61.4 (s), −143.7 (sept, $^1J_{P\text{-}F}$ = 711 Hz). ^{1}H NMR: δ (ppm) 6.20 (s, 4H, C_5H_4), 6.05 (s, 4 H, C_5H_4), 2.44 (m, 4H, $CH(CH_3)_2$), 1.27 (dd, $^3J_{H\text{-}P}$ = 18.5 Hz, $^3J_{H\text{-}H}$ = 6.78 Hz, 12H, $CH(CH_3)_2$), 1.22 (dd, $^3J_{H\text{-}P}$ = 17.8 Hz, $^3J_{H\text{-}H}$ = 6.04 Hz, 12H, $CH(CH_3)_2$). Anal. Calcd for $C_{22}H_{36}CoF_6P_3S_2$: C, 41.91; H, 5.76. Found: C, 41.95; H, 5.36.

2.3.5. [1-dtbpcS][PF$_6$]

A solution of [1-dtbpc][PF$_6$] (0.0357 g, 0.0746 mmol) and sulfur (0.0050 g, 0.16 mmol) in $CHCl_3$ (15 mL) was refluxed overnight. Upon cooling the resulting solution was filtered via cannula. The solvent volume was reduced to approximately 5 mL *in vacuo*, and the addition of hexanes resulted in the formation of a precipitate. The resulting solution was filtered via cannula, and the filtrate was washed with hexanes (3 × 5 mL), and dried *in vacuo* to yield 0.0206 g (54% yield) of [1-dtbpcS][PF$_6$] as a yellow solid. ^{31}P NMR: δ (ppm) 74.3 (s), −143.6 (sept, $^1J_{P\text{-}F}$ = 711 Hz). ^{1}H NMR: δ (ppm) 6.11 (s, 2H, C_5H_4), 6.06 (s, 2H, C_5H_4), 5.89 (s, 5H, C_5H_5), 1.40 (d, $^3J_{H\text{-}P}$ = 16.1 Hz, 18H, $C(CH_3)_3$). Anal. Calcd for $C_{18}H_{27}CoF_6P_2S$: C, 42.36; H, 5.33. Found: C, 42.08; H, 5.56.

2.4. Preparation of phosphinoselenoyls

2.4.1. [dppcSe$_2$][PF$_6$]

A solution of [dppc][PF$_6$] (0.1500 g, 0.214 mmol) and selenium (0.0379 g, 0.480 mmol) in $CHCl_3$ (20 mL) was refluxed for 7 h. Upon cooling the solution was filtered via cannula, and the addition of Et_2O resulted in the formation of an orange precipitate. The solution was filtered via cannula and the resulting solid was dried *in vacuo* to yield 0.1252 g (68% yield) of [dppcSe$_2$][PF$_6$] as a red-orange solid. ^{31}P NMR: δ (ppm) 53.9 (s, $^1J_{P\text{-}Se}$ = 773 Hz), −143.9 (sept, $^1J_{P\text{-}F}$ = 711 Hz). ^{1}H NMR: δ (ppm) 7.62 (m, 20H, C_6H_5), 6.02 (s, 4H, C_5H_4), 5.67 (s, 4 H, C_5H_4). Anal. Calcd for $C_{34}H_{28}CoF_6P_3Se_2$: C, 47.47; H, 3.28. Found: C, 47.78; H, 3.16.

2.4.2. [dcpcSe$_2$][PF$_6$]

[dcpcSe$_2$][PF$_6$] was prepared in a similar fashion as [dcpcS$_2$][PF$_6$], using [dcpc][PF$_6$] (0.0999 g, 0.137 mmol) and selenium (0.0230 g, 0.291 mmol). A total of 0.1091 g (90% yield) of the red-orange product was obtained. ^{31}P NMR: δ (ppm) 46.4 (s, $^1J_{P\text{-}Se}$ = 736 Hz), −143.7 (sept, $^1J_{P\text{-}F}$ = 711 Hz). ^{1}H NMR: δ (ppm) 6.22 (s, 4H, C_5H_4), 6.01 (s, 4 H, C_5H_4), 2.25–1.10 (m, 44H, C_6H_{11}). Anal. Calcd for $C_{34}H_{52}CoF_6P_3Se_2$: C, 46.17; H, 5.93. Found: C, 46.03; H, 5.63.

2.4.3. dcpfSe$_2$

A solution of dcpf (0.1557 g, 0.269 mmol) and selenium (0.0599 g, 0.632 mmol) in 25 mL of chloroform was refluxed for 2 h. Upon cooling the solution was filtered via cannula and the filtrate was dried *in vacuo*. Column chromatography using 4:1 (v/v) hexanes: CH_2Cl_2 as the eluent yielded 0.0951 g (48% yield) dcpfSe$_2$

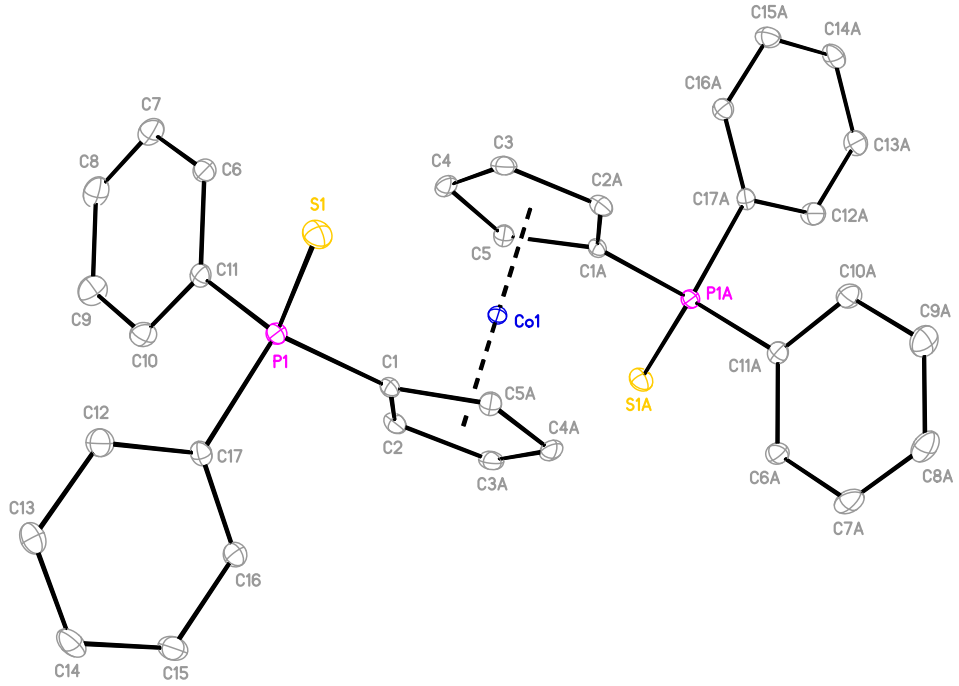

Fig. 5. Perspective view of [dppcS$_2$][PF$_6$] with 30% ellipsoids. H atoms and PF_6^- omitted for clarity.

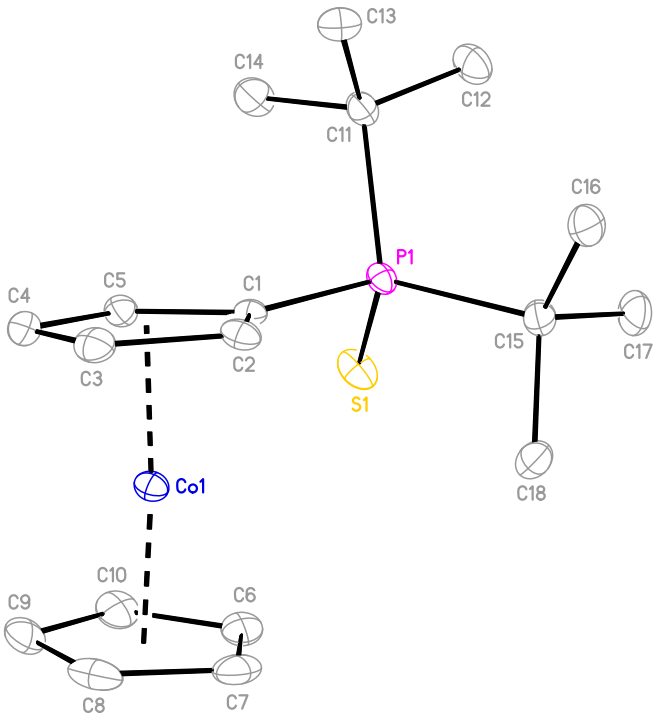

Fig. 6. Perspective view of [1-dtbpcS][PF_6] with 30% ellipsoids. H atoms and PF_6^- omitted for clarity.

as an orange solid upon removal of the solvent. ^{31}P NMR: δ (ppm) 49.9 (s, $^1J_{P\text{-}Se}$ = 710 Hz). ^1H NMR: δ (ppm) 4.80 (AA'BB', 4H, C_5H_4) 4.44 (AA'BB', 4H, C_5H_4) 1.32 (m, 44H, C_6H_{11}). Anal. Calcd for $C_{34}H_{52}FeP_2Se_2 0.5C_6H_{14}$: C, 57.01; H, 7.63. Found: C, 57.11; H, 7.68.

2.4.4. [dippcSe$_2$][PF$_6$]

[dippcSe$_2$][PF_6] was prepared in a similar fashion as [dippcS$_2$][PF_6], using [dippc][PF_6] (0.0252 g, 0.0445 mmol) and selenium

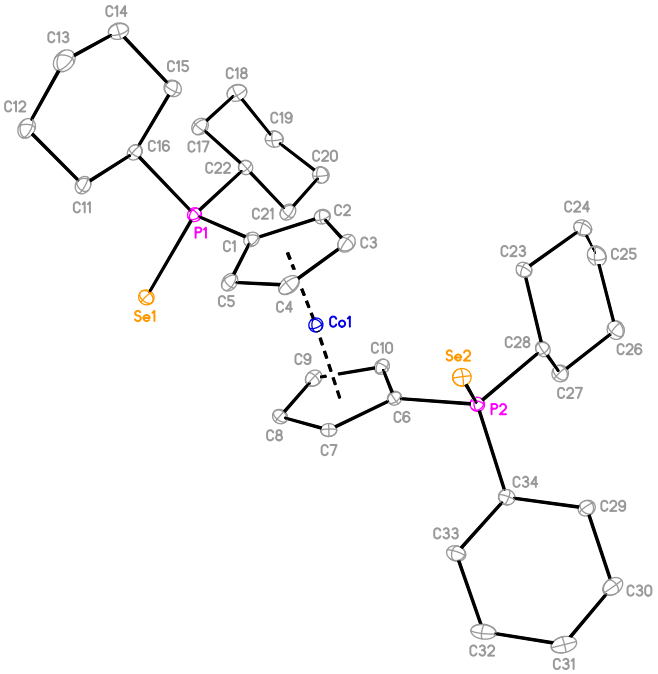

Fig. 7. Perspective view of [dcpcSe$_2$][PF_6] with 30% ellipsoids. H atoms and PF_6^- omitted for clarity.

(0.0074 g, 0.094 mmol). A total of 0.0277 g (86% yield) of the red–orange product was obtained. ^{31}P NMR: δ (ppm) 54.9 (s, $^1J_{P\text{-}Se}$ = 746 Hz), −143.7 (sept, $^1J_{P\text{-}F}$ = 711 Hz). ^1H NMR: δ (ppm) 6.23 (s, 4H, C_5H_4), 6.05 (s, 4 H, C_5H_4), 2.48 (m, 4H, $CH(CH_3)_2$), 1.26 (dd, $^3J_{H\text{-}P}$ = 14.2 Hz, $^3J_{H\text{-}H}$ = 5.68 Hz, 12H, $CH(CH_3)_2$), 1.21 (dd, $^3J_{H\text{-}P}$ = 15.2 Hz, $^3J_{H\text{-}H}$ = 7.08 Hz, 12H, $CH(CH_3)_2$). Anal. Calcd for $C_{22}H_{36}CoF_6P_3Se_2$: C, 36.48; H, 5.01. Found: C, 36.21; H, 4.96.

2.4.5. [1-dtbpcSe][PF$_6$]

A solution of [1-dtbpc][PF_6] (0.0351 g, 0.0734 mmol) and selenium (0.0092 g, 0.12 mmol) in $CHCl_3$ (15 mL) was refluxed for 2.25 h. The solution was filtered via cannula and the volume of solvent was reduced to approximately 5 mL *in vacuo*. The addition of Et_2O resulted in the formation of a precipitate. The resulting solution was filtered via cannula, and the remaining solid was washed with hexanes (3 × 5 mL), and dried *in vacuo* to yield 0.283 (69% yield) of [1-dtbpcSe][PF_6] as a yellow-orange solid. ^{31}P NMR: δ (ppm) 70.8 (s, $^1J_{P\text{-}Se}$ = 731 Hz), −143.6 (sept, $^1J_{P\text{-}F}$ = 711 Hz). ^1H NMR: δ (ppm) 6.12 (s, 2H, C_5H_4), 6.10 (s, 2H, C_5H_4), 5.91 (s, 5H, C_5H_5), 1.43 (d, $^3J_{H\text{-}P}$ = 16.5 Hz, 18H, $C(CH_3)_3$). Anal. Calcd for $C_{18}H_{27}CoF_6P_2Se$: C, 38.79; H, 4.88. Found: C, 38.40; H, 4.51.

2.5. Preparation of transition metal complexes

2.5.1. [PdCl$_2$(dppc)][PF$_6$]

A solution of [dppc][PF_6] (0.1194 g, 0.170 mmol) and [$PdCl_2(CH_3CN)_2$] (0.0445 g, 0.172 mmol) in CH_2Cl_2 (25 mL) was stirred overnight at ambient temperature, resulting in the formation of a yellow precipitate. The solution was filtered via cannula. The solid was washed with Et_2O (3 × 5 mL), and dried *in vacuo* yielding 0.0108 g (72% yield) of the product as a yellow solid. ^{31}P NMR (CD_3NO_2): δ (ppm) 28.6 (s), −144.1 (sept, $^1J_{P\text{-}F}$ = 707 Hz). ^1H NMR (CD_3NO_2): δ (ppm) 7.86 (m, 20H, C_6H_5), 5.93 (s, 4H, C_5H_4), 5.90 (s, 4 H, C_5H_4). Anal. Calcd for $C_{34}H_{28}Cl_2CoF_6P_3Pd{\cdot}0.5\ CH_2Cl_2$: C, 44.93; H, 3.17. Found: C, 45.11; H, 2.86.

2.5.2. [PdCl$_2$(dcpc)][PF$_6$]

A solution of [dcpc][PF_6] (0.1000 g, 0.138 mmol) and [$PdCl_2(CH_3CN)_2$] (0.0371 g, 0.143 mmol) in CH_2Cl_2 (20 mL) was stirred at ambient temperature overnight, resulting in the formation of a precipitate. The solution was filtered via cannula, and the volume of solvent was reduced to approximately 5 mL *in vacuo*. The addition of Et_2O resulted in the formation of a precipitate. The resulting solution was filtered via cannula, and the remaining solid was washed with Et_2O (3 × 5 mL), and dried *in vacuo*. A total of 0.0599 g (48% yield) of the yellow product was obtained. ^{31}P NMR (CD_2Cl_2): δ (ppm) 48.6 (s), −1143.7 (sept, $^1J_{P\text{-}F}$ = 711 Hz). ^1H NMR (CD_2Cl_2): δ (ppm) 6.03 (s, 4H, C_5H_4), 5.98 (s, 4 H, C_5H_4), 2.79 (br, 4H, C_6H_{11}), 2.36 (br, 4H, C_6H_{11}), 1.84 (m, 20H, C_6H_{11}), 1.38 (m, 16H, C_6H_{11}). Anal. Calcd for $C_{34}H_{52}Cl_2CoF_6P_3Pd$: C, 45.18; H, 5.80. Found: C, 45.53; H, 5.99.

2.5.3. [PdCl$_2$(dippc)][PF$_6$]

A solution of [dippc][PF_6] (0.0268 g, 0.0473 mmol) and [$PdCl_2(CH_3CN)_2$] (0.0123 g, 0.0474 mmol) in CH_2Cl_2 (10 mL) was stirred overnight at ambient temperature, resulting in the formation of a yellow precipitate. The solution was filtered via cannula, and the remaining solid was washed with Et_2O (3 × 5 mL), and dried *in vacuo*. A total of 0.0151 g (43% yield) of the yellow product was obtained. ^{31}P NMR (CD_3NO_2): δ (ppm) 58.1 (s), −144.1 (sept, $^1J_{P\text{-}F}$ = 707 Hz). ^1H NMR (CD_3NO_2): δ (ppm) 6.24 (s, 4H, C_5H_4), 6.08 (s, 4 H, C_5H_4), 3.11 (m, 4H, $CH(CH_3)_2$), 1.62 (dd, $^3J_{H\text{-}P}$ = 17.6 Hz, $^3J_{H\text{-}H}$ = 6.96 Hz, 12H, $CH(CH_3)_2$), 1.31 (dd, $^3J_{H\text{-}P}$ = 16.5Hz, $^3J_{H\text{-}H}$ = 6.60 Hz, 12H, $CH(CH_3)_2$). Anal. Calcd for $C_{22}H_{36}Cl_2CoF_6P_3Pd$: C, 35.53; H, 4.88. Found: C, 35.50; H, 4.75.

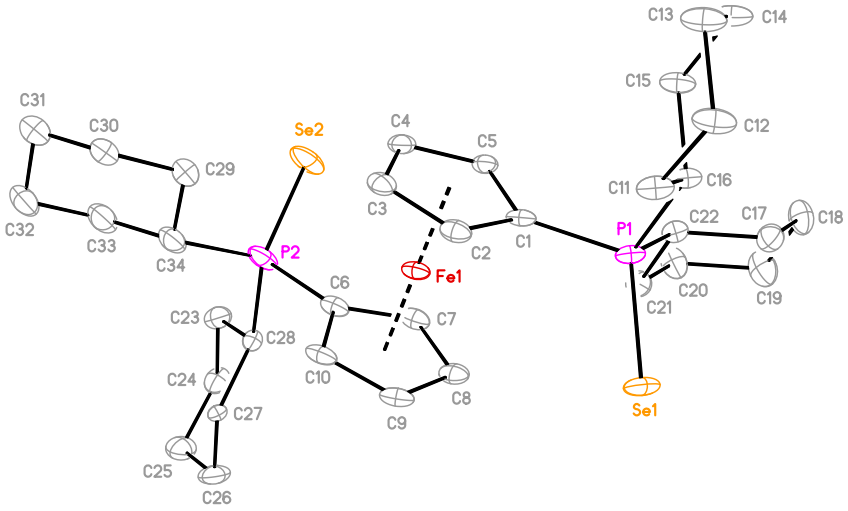

Fig. 8. Perspective view of dcpfSe_2 with 30% ellipsoids. H atoms omitted for clarity.

2.5.4. *[$PtCl_2$(dppc)][PF_6]*

[$PtCl_2$(dppc)][PF_6] was prepared according to the literature procedure; however the only characterization of the compound was the crystal structure [23]. ^{31}P NMR (CD_3NO_2): δ (ppm) 9.3 (s, $^1J_{P\text{-}Pt}$ = 3742 Hz), −144.1 (sept, $^1J_{P\text{-}F}$ = 707 Hz). ^{1}H NMR (CD_3NO_2): δ (ppm) 7.80 (m, 20H, C_6H_5), 5.92 (s, 4H, C_5H_4), 5.84 (s, 4 H, C_5H_4). Anal. Calcd for $C_{34}H_{28}Cl_2CoF_6P_3Pt$: C, 42.17; H, 2.91. Found: C, 42.02; H, 2.54.

2.5.5. *[$PtCl_2$(dcpc)][PF_6]*

A solution of [dcpc][PF_6] (0.1001 g, 0.138 mmol) and [$PtCl_2(CH_3CN)_2$] (0.0493 g, 0.142 mmol) in CH_2Cl_2 (20 mL) was stirred at ambient temperature overnight, resulting in a yellow solution. The volume of solvent was reduced to approximately 5 mL *in vacuo*, and the addition of Et_2O resulted in the formation of a precipitate. The solution was filtered via cannula, and the resulting solid was washed with Et_2O (3 × 5 mL), and dried *in vacuo*. The yellow product was collected giving 0.1151 g (84% yield). ^{31}P NMR: δ (ppm) 20.5 (s, $^1J_{P\text{-}Pt}$ = 3711 Hz), −143.6 (sept, $^1J_{P\text{-}F}$ = 711 Hz). ^{1}H NMR: δ (ppm) 6.15 (s, 4H, C_5H_4), 5.92 (s, 4 H, C_5H_4), 2.81 (br, 4H, C_6H_{11}), 2.37 (br, 4H, C_6H_{11}), 1.84 (m, 20H, C_6H_{11}), 1.38 (m, 16H, C_6H_{11}). Anal. Calcd for $C_{34}H_{52}Cl_2CoF_6P_3Pd$: C, 41.14; H, 5.28. Found: C, 40.98; H, 5.05.

2.5.6. *[$PtCl_2$(dippc)][PF_6]*

[$PtCl_2$(dippc)][PF_6] was prepared in a similar fashion as [$PdCl_2$(dippc)][PF_6], using [dippc][PF_6] (0.0260 g, 0.0459 mmol) and [$PtCl_2(CH_3CN)_2$] (0.0160 g, 0.0460 mmol). A total of 0.0115 g (30% yield) of the yellow product was collected. ^{31}P NMR (CD_3NO_2): δ (ppm) 29.0 (s, $^1J_{P\text{-}Pt}$ = 3731 Hz), −144.0 (sept, $^1J_{P\text{-}F}$ = 707 Hz). ^{1}H NMR (CD_3NO_2): δ (ppm) 6.15 (s, 4H, C_5H_4), 6.07 (s, 4 H, C_5H_4), 3.13 (m, 4H, $CH(CH_3)_2$), 1.56 (dd, $^3J_{H\text{-}P}$ = 17.8 Hz, $^3J_{H\text{-}H}$ = 7.14 Hz, 12H, $CH(CH_3)_2$), 1.27 (dd, $^3J_{H\text{-}P}$ = 17.2 Hz, $^3J_{H\text{-}H}$ = 6.96 Hz, 12H, $CH(CH_3)_2$). Anal. Calcd for $C_{22}H_{36}Cl_2CoF_6P_3Pd$: C, 31.75; H, 4.36. Found: C, 31.84; H, 4.57.

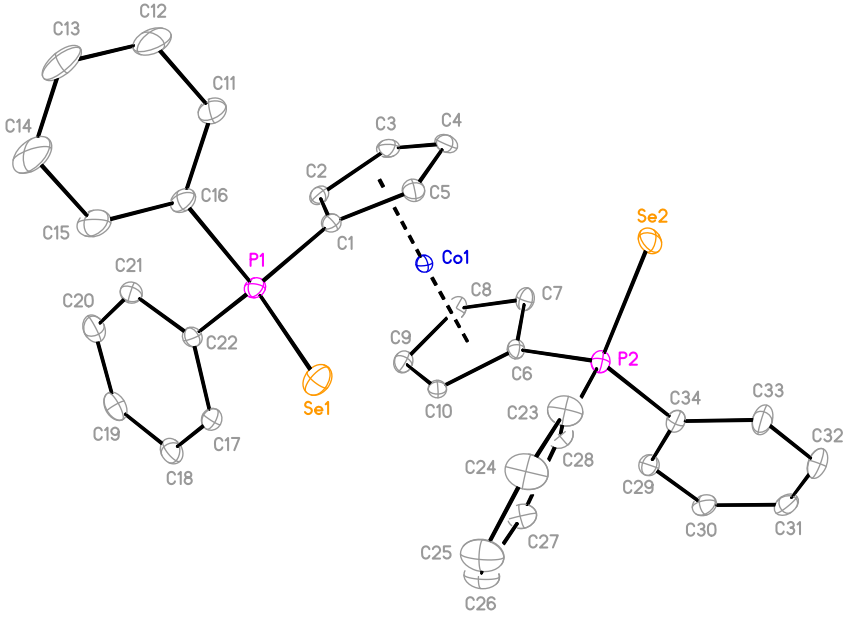

Fig. 9. CV Perspective view of [dppcSe_2][PF_6] with 30% ellipsoids. H atoms and PF_6^- omitted for clarity.

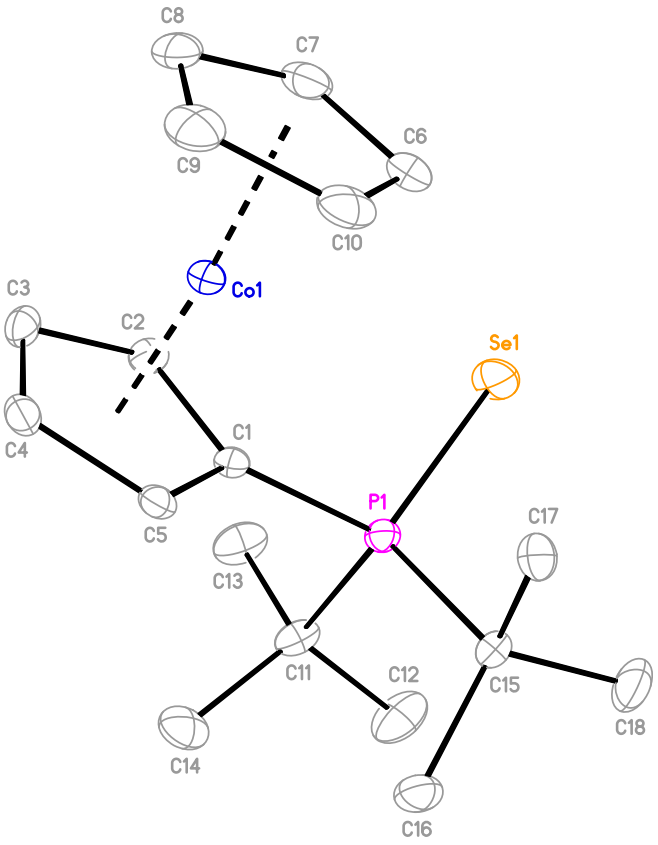

Fig. 10. Perspective view of [1-dtbpcSe][PF_6] with 30% ellipsoids. H atoms and PF_6^- omitted for clarity.

2.6. Electrochemical procedures

For all cyclic voltammetry experiments, scans were conducted at ambient temperature (22 ± 1 °C) using a PAR 263A potentiostat/galvanostat under an argon atmosphere. Solutions of analyte (1.0 mM) in CH_2Cl_2 (10.0 mL) were examined, with [NBu_4][PF_6] (0.1 M) serving as the supporting electrolyte. Voltammograms of [$PdCl_2$(dippc)][PF_6] and [$PtCl_2$(dippc)][PF_6] were recorded under similar conditions in nitromethane (10.0 mL). Scan rates were conducted at 50 and 100–1000 mV/s, in 100 mV/s increments, and recorded via PowerSuite software. Background scans of [NBu_4][PF_6] were subtracted for the 100 mV/s scan rate. A 1.5 mm glassy carbon disc, which was polished with 1.0 μm then 0.25 μm diamond pastes and rinsed with CH_2Cl_2 prior to use, served as the working electrode. A platinum wire served as the counter electrode, and Ag/AgCl, separated from solution by an E-porosity glass frit, served as the reference electrode. Ferrocene (1.0 mM) was added as a reference at the end of all experiments.

2.7. Crystallographic procedures

Crystals of the phosphinothioyls and phosphinoselenoyls, with the exception of [$dppcSe_2$][PF_6], suitable for X-ray analysis were obtained by slow diffusion of hexanes into a solution of the desired compound in CH_2Cl_2 in a freezer. Slow diffusion of Et_2O into a solution of [$dppcSe_2$][PF_6] in CH_2Cl_2 in a freezer was utilized for growing crystals of this compound. Crystals of [Au_2Cl_2(dppc)][PF_6] were obtained by slow diffusion of di-iso-propyl ether into a solution of [Au_2Cl_2(dppc)][PF_6] in 1,2-dichloroethane in a refrigerator. The crystals were mounted using NVH immersion oil onto a nylon fiber and cooled to the data collection temperature. Data were collected on a Brüker-AXS Kappa APEX II CCD diffractometer with 0.71073 Å Mo-K_α radiation for the phosphinothioyls (Table 1), phosphinoselenoyls (Table 2) and [Au_2Cl_2(dppc)][PF_6] (Table 3). Unit cell parameters were obtained from 90 data frames, 0.3° Φ, from three different sections of the Ewald sphere. Using SHELXS-97, direct methods were employed to solve the structures and refinement was performed by full-matrix least-square procedures on F^2 [24]. The diffraction data were consistent with the assigned space groups. The data-sets were treated with SADABS absorption corrections based on redundant multi-scan data [25]. All non-hydrogen atoms were refined with anisotropic displacement parameters. All hydrogen atoms were treated as idealized contributions.

For [$dcpcS_2$][PF_6] the asymmetric unit contains one $[CoL]^+$ cation, one $[PF_6]^-$ anion and two molecules of CH_2Cl_2 solvent all located on general positions yielding $Z = 2$, and $Z' = 1$. For [$dcpcSe_2$][PF_6] the asymmetric unit contains 1.5 $[dcpcSe_2]^+$ cations, 1.5 $[PF_6]^-$ anions and 1.5 molecules of CH_2Cl_2 solvent yielding $Z = 4$, and $Z' = 1.5$. The CH_2Cl_2 solvent molecules were both disordered. The full molecule was modeled over two positions but the half molecule was disordered over a symmetry element and was SQUEEZED out of the refinement [26]. The SQUEEZE results were consistent with this model [26]. For [Au_2Cl_2(dppc)][PF_6] the asymmetric unit contains one $[Au_2Cl_2(dppc)]^+$ cation, one $[PF_6]^-$ anion, and four molecules of dichloroethane solvent all located on general positions yielding $Z = 4$, and $Z' = 1$. Three out of the four solvent molecules were disordered, so the solvent was removed with SQUEEZE [26]. The SQUEEZE results were consistent with this model [26].

3. Results and discussion

The phosphinocobaltocenium compounds employed in this study were prepared according to the literature preparations [13,21]. However, using the literature synthesis we were unable to prepare 1,1′-bis(di-tert-butylphosphino)cobaltocenium and thus it is not included in this report [21]. In the course of preparing [dppc][PF_6] X-ray quality crystals were obtained. As the structures of [dppc][BF_4] [27] and [dppc][NO_3] [14] have previously been reported, this structure is included in the supporting information.

Table 5
Selected bond lengths (Å) and angles (°) for phosphinochalcogenyl cobaltocenium and phosphinochalcogenyl ferrocene compounds.

	[$dppcO_2$][PF_6]	$dppfO_2$	[$dppcS_2$][PF_6]	$dppfS_2$	[$dppcSe_2$][PF_6]	$dppfSe_2$	[$dcpcS_2$][PF_6]	$dcpfS_2$	[$dcpcSe_2$][PF_6]	$dcpfSe_2$	[1-dtbpcS][PF_6]	[1-dtbpcSe][PF_6]
P-E (avg.)	1.464	1.493	1.9425	1.938	2.0679	2.103	1.9528	1.9608	2.1076	2.1195	1.9503(8)	2.1089(6)
M-C (avg.)	2.032	2.046	2.0346	2.039	2.017	2.044	2.0426	2.0508	2.040	2.048	2.027	2.030
τ[a]	177.69	180.00	180.00	180.00	84.50	180.00	88.14	151.85	145.02	150.07		
θ[b]	0.22	0.00	0.00	0.00	4.09	0.00	5.83	2.04	5.88	1.09		
δ_P[c] (avg.)	0.076	−0.011	−0.105	−0.035	−0.075	−0.148	−0.118	−0.159	−0.160	−0.242		
Reference	[18]	[35]		[36]		[37]						

[a] The torsion angle C_A-X_A-X_B-C_B where C is the carbon atom bonded to phosphorus and X is the centroid of the C_5 ring.
[b] The dihedral angle between the two C_5 rings.
[c] Average deviation of the P atoms from the C_5 planes; a positive value indicates P is closer to Co/Fe.

Table 6
$\%V_{bur}$ values for phosphinochalcogenyls with cobaltocenium and ferrocene backbones. Values in parentheses are the average deviation from the mean for the two values.

Cobaltocenium			Ferrocene		
Compound	$\%V_{bur}$	Reference	Compound	$\%V_{bur}$	Reference
$[dppcO_2][PF_6]$		[35][a]	$dppfO_2$	51.7(0.0)	[36][b]
$[dppcS_2][PF_6]$	38.9(0.0)	this work	$dppfS_2$	40.5(0.0)	[41]
$[dppcSe_2][PF_6]$	45.8(5.4)	this work	$dppfSe_2$	37.3(0.0)	[41]
$[dcpcS_2][PF_6]$	48.2(5.8)	this work	$dcpfS_2$	42.4(0.2)	this work
$[dcpcSe_2][PF_6]$	40.2(1.1)[c]	this work	$dcpfSe_2$	39.2(0.2)	this work
$[dippcO_2][PF_6]$			$dippfO_2$[d]	51.9(0.9)	[42][b]
$[dippcS_2][PF_6]$			$dippfS_2$[d]	41.4(0.1)	[42][b]
$[dippcSe_2][PF_6]$			$dippfSe_2$[d]	39.6(1.2)	[42][b]
[1-dtbpcS][PF_6]	45.3	this work	dtbpfS[e]		
[1-dtbpcSe][PF_6]	42.8	this work	dtbpfSe[e]		
$[dtbpcSe_2][PF_6]$			$dtbpfSe_2$[e]	42.6(0.4)	[41]

[a] While the structure of this compound has been published, the R-factor was greater than 7% which has been suggested as the cutoff [39].
[b] Reference to the published structure; the $\%V_{bur}$ was calculated in this work.
[c] The average deviation from the mean is for four values as there are two crystallographically independent $[dcpcSe_2]^+$ in the unit cell.
[d] dippf = 1,1′-bis(di-iso-propylphosphino)ferrocene.
[e] dtbpf = 1,1′-bis(di-tert-butylphosphino)ferrocene.

The electrochemistry of the phosphinocobaltocenium compounds was examined in CH_2Cl_2 using $[NBu_4][PF_6]$ as the supporting electrolyte. Each compound exhibited a reversible reductive wave at potentials significantly more negative than that of ferrocene (Table 4). The phosphine substituents have been found to be less electron donating than a hydrogen in the oxidative electrochemistry of the analogous bis(phosphino)ferrocene compounds. Therefore the reduction potentials for the phosphinocobaltocenium compounds are more positive than that of cobaltocenium. In addition, the bis(phosphino)cobaltocenium compounds exhibited an irreversible reductive wave at more negative potentials (Fig. 2). This is likely due to the Co(I)/Co(II) couple which is prone to dissociation of a cyclopentadienyl ring [1,16,17].

The phosphine oxide, $[dppcO_2][PF_6]$, was prepared in high yield using a new procedure. This method circumvents the previous requirement of freshly prepared peracetic acid and organic extractions, and allows for faster isolation of the product as an overnight recrystallization was eliminated [18]. Pure $[dppcO_2][PF_6]$ was isolated as a yellow solid using this new procedure despite being previously reported as a black crystalline solid [18].

Table 7
Potentials (V vs. $FcH^{0/+}$ in CH_2Cl_2 with $[NBu_4][PF_6]$ as the supporting electrolyte) and potential differences ($\Delta E = E_{phosphinochalcogenyl} - E_{phosphine}$) of the phosphinochalcogenyl.

Compound	E_1°	ΔE_1	E_2°	ΔE_2	$E_p^{Ox\ 1}$	E_p^{Red}	E_{Fe}°
$[dppcO_2][PF_6]$	−0.85	0.28	−1.92	0.40			
$[dppcS_2][PF_6]$	−0.82	0.31	−1.90	0.42			
$[dcpcS_2][PF_6]$	−0.90	0.37	−1.99	0.42			
$dcpfS_2$							0.37
$[dippcS_2][PF_6]$	−0.89	0.36	−2.01	0.37			
[1-dtbpcS][PF_6]	−1.11	0.17	−2.20				
$[dppcSe_2][PF_6]$	−0.80	0.34	−1.89	0.43	0.84		
$dppfSe_2$					0.32	−0.14	1.10[a]
$[dcpcSe_2][PF_6]$	−0.87	0.40	−1.96	0.45	0.79	−0.09	
$dcpfSe_2$					0.27	−0.04	1.03[a]
$[dippcSe_2][PF_6]$	−0.85	0.40	−1.96	0.42	0.71	0.05	
$dippfSe_2$					0.21	−0.24	1.00[a]
[1-dtbpcSe][PF_6]	−1.10	0.18	−2.18				
$dtbpfSe_2$					0.24	−0.07	1.06[a]

[a] The reduction wave has a significantly larger peak current than the oxidative wave suggesting deposition of the electrochemically generated trication.

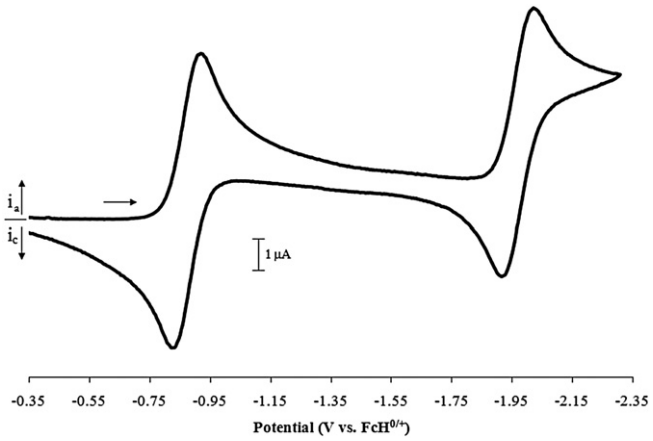

Fig. 11. CV scan for the reduction of 1.0 mM $[dcpcSe_2][PF_6]$ in CH_2Cl_2 with 0.1 M $[NBu_4][PF_6]$ as the supporting electrolyte at 100 mV/s.

Using methods adapted from the analogous bis(phosphino) ferrocenes [34], eight new phosphinothioyls ($[dppcS_2][PF_6]$, $[dcpcS_2][PF_6]$, $[dippcS_2][PF_6]$, [1-dtbpcS][PF_6]) and phosphinoselenoyls ($[dppcSe_2][PF_6]$, $[dcpcSe_2][PF_6]$, $[dippcSe_2][PF_6]$, [1-dtbpcSe][PF_6]) were prepared in moderate to high yield. The compounds were characterized by ^1H and $^{31}P\{^1H\}$ NMR. The signals in the ^{31}P spectra showed the anticipated downfield shift upon addition of the chalcogen. In order to compare these cobalt complexes to their iron analogues, $dcpfS_2$ and $dcpfSe_2$ were prepared and characterized by ^1H and $^{31}P\{^1H\}$ NMR. Crystals suitable for X-ray analysis were obtained for eight of these compounds. The structures of $[dcpcS_2][PF_6]$ (Fig. 3), $dcpfS_2$ (Fig. 4), $[dppcS_2][PF_6]$ (Fig. 5), [1-dtbpcS][PF_6] (Fig. 6), $[dcpcSe_2][PF_6]$ (Fig. 7), $dcpfSe_2$ (Fig. 8), $[dppcSe_2][PF_6]$ (Fig. 9) and [1-dtbpcSe][PF_6] (Fig. 10) are reported herein. Selected bond lengths and angles are presented in Table 5. The P = E bond lengths are generally shorter in the cobalt compounds as compared to the iron analogues. In addition, the P = E bonds are slightly longer when comparing cyclohexyl substituted compounds to their phenyl substituted analogs.

Recently, the percent buried volume ($\%V_{bur}$) has been proposed as an effective means of describing the overall steric parameters of ligands [38]. Defined as the percent of the total volume of a sphere occupied by a ligand around a central atom, $\%V_{bur}$ relies on crystallographic data and has been shown to correlate well with the Tolman cone angle of free tertiary phosphine ligands and linear $[(R_3P)AuCl]$ complexes [39]. Calculations with bidentate phosphine

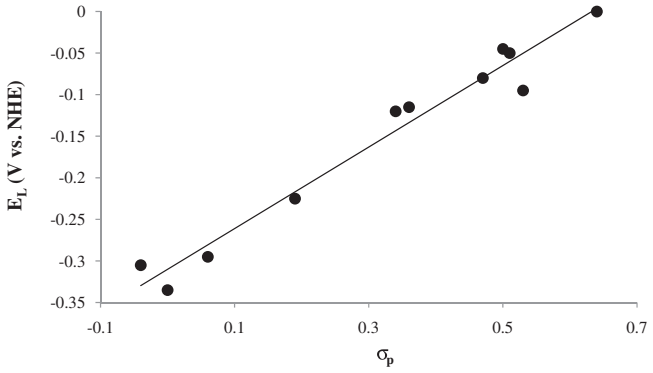

Fig. 12. Relationship between the E_L values of 1,1′-bis(substituted)cobaltocenium complexes obtained in CH_2Cl_2 with the Hammett parameter (σ_p) of the substituents. $E_L = 0.4902(\sigma_p) - 0.3100$, $R^2 = 0.9645$.

ligands were also found to agree well with Tolman's prior work [39]. We have shown that a correlation exists between θ and $\%V_{bur}$ for simple monodentate phosphinochalcogenyls and have performed $\%V_{bur}$ calculations on 1,1′-bis(phosphinochalcogenyl)ferrocene compounds [40]. The $\%V_{bur}$ values have been calculated for the cobaltocenium species and compared to the ferrocene analogues (Table 6).

However, meaningful comparisons between the ferrocene and cobaltocenium compounds cannot be made due to the large differences in $\%V_{bur}$ for each phosphorus atom in the same molecule. These large differences, in particular in the cobaltocenium compounds, can be seen as the average deviation from the mean. The general trend for the phosphinochalcogenyl ferrocene compounds is that the $\%V_{bur}$ values decrease substantially on going from O to S and slightly from S to Se. In addition, the size of the R groups on the phosphorus are important as the $\%V_{bur}$ values are Ph < Cy ≈ ^{i}Pr < ^{t}Bu for the ferrocene compounds. The trends are not as straightforward in the cobaltocenium analogues.

The electrochemistry of each of the cobaltocenium phosphinochalcogenyls was also examined (Table 7). Two reversible reductive waves were observed for each cobaltocenium compound at all scan rates (Fig. 11). The first wave, E_1°, can be attributed to the Co(II/III) couple while the second, E_2°, is likely due to the Co(I/II) couple. The reversibility of E_2° suggests that the chalcogenides stabilize the formation of an anionic cobaltocene species on the CV timescale. Similar reversibility of the Co(I/II) couple was noted for several metal carbonyl complexes containing dppc$^+$ and was attributed to a stabilizing template effect where bidentate coordination of dppc$^+$ to a metal center prevented reactions of the electrochemically generated Co(I) species [1,16,17]. The reversibility of E_2° for the phosphinochalcogenyls is interesting. Similar to the instability of the electrochemically generated dppf$^+$ [30], it would seem that the presence of lone pair on the phosphorus of phosphine cobaltocenium compounds destabilized the Co(I) species.

The electrochemical parameter (E_L) has been defined for disubstituted sandwhich compounds as $1/2E^\circ$ vs. SHE [43]. A correlation exists between E_L for the E_1° reduction potentials of the 1,1′-bis(substituted)cobaltocenium complexes and the known Hammett substituent constants (σ_p) for the corresponding substituents (Fig. 12) [28,31,34]. This correlation suggests that the electronic nature of the substituents is directly proportional to the reduction potential, allowing for the prediction of E_1° reduction potentials of 1,1′-bis(substituted)cobaltocenium complexes based on σ_p values. Previous estimates of the Hammett parameters for the −P(Se)Ph$_2$ and −P(Se)^{i}Pr$_2$ functional groups [34] using the redox potential of the 1,1′-bis(substituted)ferrocene compounds were based on the incorrect assumption that the oxidation occurred at the iron center and thus the correlation between σ_p and the iron redox potential held [33]. Using the data for the 1,1′-bis(substituted)cobaltocenium complexes, estimates for the σ_p values for the −P(Se)Ph$_2$, −P(Se)Cy$_2$, and −P(Se)^{i}Pr$_2$ functional groups are 0.49, 0.42, and 0.44 respectively.

Oxidative sweeps of [dppcSe$_2$][PF$_6$], [dcpcSe$_2$][PF$_6$], and [dippcSe$_2$][PF$_6$] exhibited an electrochemically irreversible oxidation, followed by the reduction of an electrochemically generated product (Fig. 13). Previous electrochemical experiments with dppfSe$_2$ and dippfSe$_2$ produced similar results [34], although oxidation occurred at potentials approximately 0.5 V less positive than the cobaltocenium analogues. As the cobaltocenium compounds are initially cationic, the difference in the potentials at which oxidation occurs is anticipated. The same trend is observed in the oxidation of [dcpcSe$_2$][PF$_6$] as compared to dcpfSe$_2$. Oxidation of dtbpfSe$_2$ was shown to be a two-electron process that resulted in the formation of [dtbpfSe$_2$][BF$_4$]$_2$ in which there had been intramolecular Se–Se bond formation [33]. A similar process

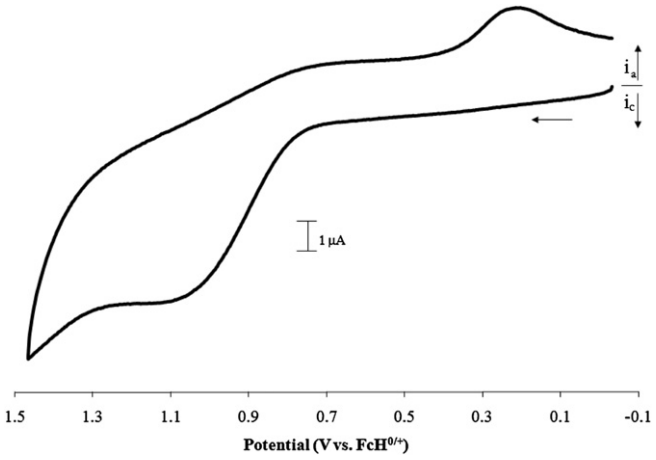

Fig. 13. CV for the oxidation of 1.0 mM [dcpcSe$_2$][PF$_6$] in CH$_2$Cl$_2$ with 0.1 M [NBu$_4$][PF$_6$] as the supporting electrolyte at 100 mV/s.

may also be occurring for the phosphinoselenoyl cobaltocenium species which would result in the formation of a trication. Interestingly, a reductive wave was not observed following the oxidation of [dppcSe$_2$][PF$_6$], which may be attributable to the limited solubility exhibited by many [dppc][PF$_6$] compounds (*vide infra*). The ferrocene derivatives also display an oxidation at approximately 1 V vs. FcH$^{0/+}$ which can be attributed to oxidation of the iron center.

In addition to the phosphinochalcogenyls, several transition metal complexes with 1,1′-bis(phosphino)cobaltocenium ligands were prepared in moderate yields using methods previously established for 1,1′-bis(phosphino)ferrocenes [30–33]. Unlike

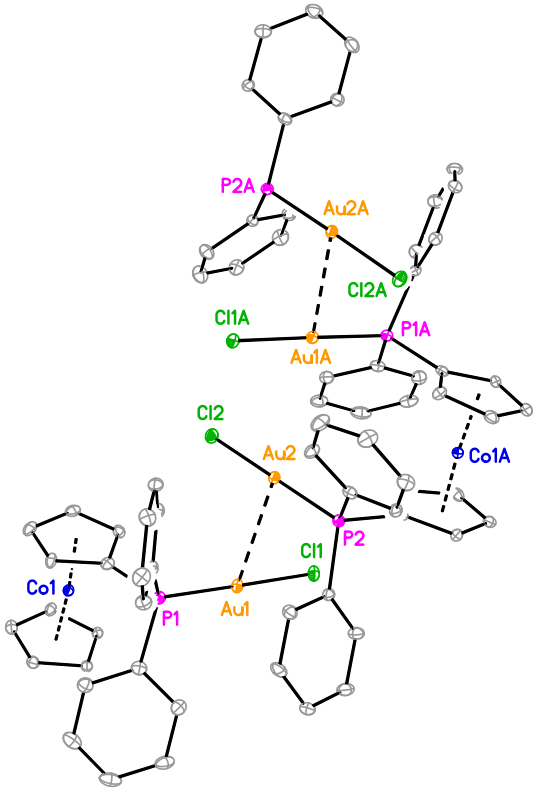

Fig. 14. Perspective view of [Au$_2$Cl$_2$(dppc)][PF$_6$] with 30% ellipsoids. H atoms and PF$_6^-$ omitted for clarity.

Table 8
Selected bond lengths (Å) and angles (°) for $[Au_2Cl_2(dppc)][PF_6]$ and $[Au_2Cl_2(dppf)]$.

	$[Au_2Cl_2(dppc)][PF_6]$	$[Au_2Cl_2(dppf)]$[a]
Space group	$P2_1/n$	$P\bar{1}$
P–Au	2.2404[b]	2.239(3), 2.229[b]
Au–Cl	2.3076[b]	2.300(3), 2.226[b]
M–C (avg.)	2.052	2.04, 2.06
Au–Au	3.0873(2)	3.083(1)
P–Au–Cl	178.91[b]	176.0(1), 174.4[b]
τ[c]	74.44	180.00, 124.18
θ[d]	4.93	0.00, 3.17
δ_P[e] (avg.)	0.059	0.061, −0.038
Solvent	$4C_2H_4Cl_2$	$2/3\ CHCl_3$
Reference		[39]

[a] The structure has two crystallographically independent molecules in the unit cell.
[b] Average value.
[c] The torsion angle C_A-X_A-X_B-C_B where C is the carbon atom bonded to phosphorus and X is the centroid of the C_5 ring.
[d] The dihedral angle between the two C_5 rings.
[e] Average deviation of the P atoms from the C_5 planes; a positive value indicates P is closer to Co/Fe.

analogous ferrocene complexes, $[MCl_2(dppc)][PF_6]$ (M = Pd or Pt) precipitated from solution, and were found to be insoluble in all but very polar organic solvents such as DMF and nitromethane. Similarly, $[MCl_2(dippc)][PF_6]$ (M = Pd or Pt) is sparingly soluble in CH_2Cl_2 while $[MCl_2(dcpc)][PF_6]$ (M = Pd or Pt) is quite soluble in CH_2Cl_2. Clearly the phosphine substituents contribute significantly to the solubility of these transition metal complexes in organic solvents. Alkyl groups appear to impart increased solubility over phenyl groups. These observations may provide insight into the observation that recycling a $[PdCl_2(P^{\cap}P)][PF_6]$ ($P^{\cap}P$ = dcpc, dippc or dtbpc) catalytic system in $[BMIM][PF_6]$ after extracting the products with an organic solvent resulted in significant loss of activity after the second trial [21].

The structure of $[Au_2Cl_2(dppc)][PF_6]$ was determined (Fig. 14). Selected structural parameters for $[Au_2Cl_2(dppc)][PF_6]$ are presented in Table 8. The solid-state structure is a long chain of cations, linked through 3.0873 Å Au–Au interactions, which follow the screw axis. Six structures of the analogous $[Au_2Cl_2(dppf)]$ have been determined: three different polymorphs of $[Au_2Cl_2(dppf)]$ [44–46] as well as $[Au_2Cl_2(dppf)]\cdot 2/3\ CHCl_3$ [47], $[Au_2Cl_2(dppf)]\cdot 2\ CH_2Cl_2$ [48] and $[Au_2Cl_2(dppf)]\cdot CHCl_3^1/2C_6H_{14}$ [41]. Only the $[Au_2Cl_2(dppf)]\cdot 2/3\ CHCl_3$ structure exhibits an intermolecular Au–Au distance similar to that found for $[Au_2Cl_2(dppc)][PF_6]$. The synclinical eclipsed [2,49] geometry found in $[Au_2Cl_2(dppc)][PF_6]$ allows for a short intramolecular Au–Au distance of 3.666 Å. The Au–P and Au–Cl bond lengths are slightly longer and the P–Au–Cl angle is closer to 180° in $[Au_2Cl_2(dppc)][PF_6]$ as compared to $[Au_2Cl_2(dppf)]$.

The $\%V_{bur}$ can be calculated to structurally compare 1,1′-bis(phosphino)cobaltocenium ligands with the iron analogues. The $\%V_{bur}$ for the dppf ligand in one structure of $[Au_2Cl_2(dppf)]$ [45] has been calculated as 38.7 at a distance of 2.00 Å and 33.5 at 2.28 Å [36]. The $\%V_{bur}$ for the dppf ligand is 40.6 (average deviation from the mean of 0.9) at a distance of 2.00 Å and 35.3 (average deviation from the mean of 0.9) at 2.28 Å when all of the reported structures of $[Au_2Cl_2(dppf)]$ are considered. The $\%V_{bur}$ for the dppc ligand is similar, 38.5 (average deviation from the mean 3.1) at a distance of 2.00 Å and 33.6 (average deviation from the mean 3.2) at 2.28 Å. Similar to the chalcogenides, a large average deviation from the mean for the $\%V_{bur}$ of the cobaltocenium compounds was observed. Even in the structures of $[Au_2Cl_2(dppf)]$ that are not symmetric about the iron atoms [41,47], the average deviation from the mean for the $\%V_{bur}$ values is only 0.8. The reason for the differences in the cobalt compounds is unclear, but these results reinforce the warning of *caveat emptor* in regard to $\%V_{bur}$ calculations [39].

The only $[MCl_2(P^{\cap}P)][PF_6]$ structure containing a 1,1′-bis(phosphino)cobaltocenium ligand reported is $[PtCl_2(dppc)][PF_6]$ [23]. The $\%V_{bur}$ calculation for a bidentate ligand does not treat the phosphorus atoms separately [39]. The calculated $\%V_{bur}$ for the dppc ligand in this compound is 54.9. This is slightly less than the $\%V_{bur}$ for dppf in $[PtCl_2(dppf)]$ which was calculated to be 55.8 [40].

The electrochemistry of several 1,1′-bis(phosphino)cobaltocenium metal complexes was also examined (Table 9). Several unsuccessful attempts were made to examine the electrochemistry of $[PdCl_2(dppc)][PF_6]$ and $[PtCl_2(dppc)][PF_6]$. In DMF significant color changes of the solutions occurred and the experiments gave indiscernible electrochemistry. The electrochemistry of $[PdCl_2(dippc)][PF_6]$ and $[PtCl_2(dippc)][PF_6]$ had to be performed in nitromethane which gave only one reductive wave in the solvent window. The reductive wave of $[PdCl_2(dippc)][PF_6]$ was irreversible at lower scan rates and chemically reversible at higher scan rates. Cyclic voltammograms of $[PdCl_2(dcpc)][PF_6]$ and $[PtCl_2(dcpc)][PF_6]$ displayed three reductive waves, the first of which is chemically and electrochemically reversible and likely due to the Co(II/III) couple (Fig. 15). Two irreversible waves were also common to both complexes, one of which is likely due to the Co(I/II) couple. The final wave is likely due to reduction of the Pd or Pt center. An irreversible two electron reduction of the Pd in $[PdCl_2(dppf)]$ has been observed at −1.59 V vs. $FcH^{0/+}$ [50]. The bisphosphine complexes $[PtCl_2(PPh_3)_2]$ and $[PtCl_2(PEt_3)_2]$ also undergo irreversible two electron reductions of the Pt metal at −2.10 V and −2.56 V vs. $FcH^{0/+}$, respectively [51]. Comparing the $E_1°$ and $E_2°$ values of $[MCl_2(dcpc)][PF_6]$ to the phosphinochalcogenyls, $[PtCl_2(dcpc)][PF_6]$ displayed very similar reduction potentials to $[dcpcS_2][PF_6]$, suggesting that these are likely reductions of the cobalt center. Although the first reductive wave of $[PdCl_2(dcpc)][PF_6]$ is similar to that of the phosphinochalcogenyls the second reductive wave is significantly less positive suggesting that Pd is reduced at −1.64 V vs. $FcH^{0/+}$. The $[(AuCl)_2dppc][PF_6]$ and $[(AuCl)_2dcpc][PF_6]$ complexes exhibited electrochemistry (Fig. 16) resembling that of

Table 9
Potentials (V vs. $FcH^{0/+}$ in CH_2Cl_2 with $[NBu_4][PF_6]$ as the supporting electrolyte) and potential differences ($\Delta E = E_{cmpd}$-E_{phos}) for the transition metal complexes.

Compound	$E°_1$	ΔE_1	$E°_2$	ΔE_2	E_p^{red}
$[Au_2Cl_2dppc][PF_6]$	−0.66	0.48	−1.83[a]	0.49	
$[Au_2Cl_2dcpc][PF_6]$	−0.76	0.51	−1.86	0.56	
$[PdCl_2(dcpc)][PF_6]$	−0.88	0.39	−1.64[a]		−2.32
$[PtCl_2(dcpc)][PF_6]$	−0.92	0.35	−1.99[a]		−2.25
$[PdCl_2(dippc)][PF_6]$	−0.87[a,b]	0.36[c]			
$[PtCl_2(dippc)][PF_6]$	−0.89[b]	0.34[c]			

[a] Only E_p^{red} observed at 100 mV/s.
[b] Experiments were performed in nitromethane.
[c] Referenced to $[dippc][PF_6]$ examined in nitromethane.

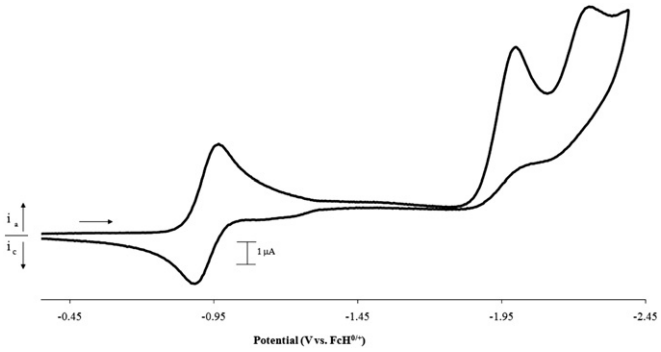

Fig. 15. CV scan for the reduction of 1.0 mM $[PtCl_2(dcpc)][PF_6]$ in CH_2Cl_2 with 0.1 M $[NBu_4][PF_6]$ as the supporting electrolyte at 100 mV/s.

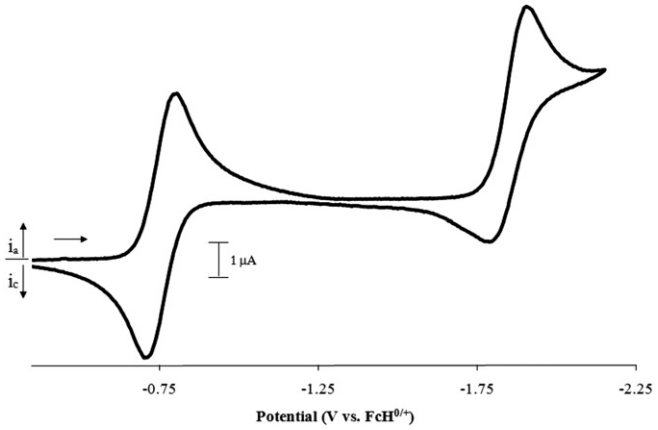

Fig. 16. CV scan for the reduction of 1.0 mM $[(AuCl)_2dcpc][PF_6]$ in CH_2Cl_2 with 0.1 M $[NBu_4][PF_6]$ as the supporting electrolyte at 100 mV/s.

the phosphinothioyls. The first reductive wave for each complex was reversible, while only $[(AuCl)_2dcpc][PF_6]$ exhibited a degree of reversibility for the second reductive wave.

With the correlation between the E_1° values of several phosphinochalcogenyls and σ_p, the question arose as to a correlation existing between the reduction potentials of cobaltocenium compounds (E_{Co}) and the potentials at which oxidation of related ferrocene compounds (E_{Fe}) occur. There are few reports of reduction potentials for 1,1′-bis(substituted)cobaltocenium compounds. Plotting the reduction potentials of the 1,1′-bis(substituted)cobaltocenium compounds versus the potential at which oxidation of the analogous ferrocene compounds occurs resulted in a linear relationship when both potentials were in CH_2Cl_2 (Fig. 17). It is worth noting that the phosphinoselenoyl species were not included as the selenium undergoes oxidation prior to the iron center. The *y*-intercept value correlates very well with the −1.33 V difference observed between the cobaltocene and ferrocene redox couples [29]. In addition, the slope suggests that the substituent effects are identical for both the 1,1′-bis(substituted) iron and cobalt species. This suggests that the redox potential of one of these species can be reasonably predicted if the potential of the analogous complex is known.

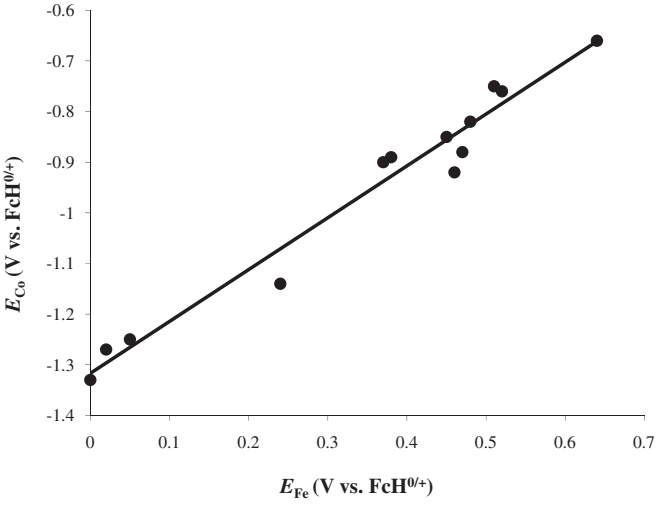

Fig. 17. Relationship between the reduction potentials of 1,1′-bis-substituted cobaltocenium species (E_{Co}) and the potential at which oxidation of the analogous ferrocene species (E_{Fe}) occurs. $E_{Co} = 1.0244(E_{Fe}) - 1.3171$, $R^2 = 0.967$.

4. Summary

Free 1,1′-bis(phosphino)cobaltocenium ligands display two reductive waves, the first of which is reversible followed by an irreversible reduction at more negative potentials. Ten new phosphinothioyls and phosphinoselenoyls were synthesized, and the X-ray structures of eight of these compounds were determined. Unlike the parent phosphines, each 1,1′-bis(phosphinochalcogenyl) cobaltocenium displays two reversible reductive waves. The electron withdrawing nature of the chalcogenides likely stabilizes the anionic complex generated upon undergoing the second reduction. The electron donating ability of the phosphine substituents appears to correlate well with the reduction potentials of 1,1′-bis(phosphino)cobaltocenium species, as evidenced by the linear relationship between σ_p and the corresponding reduction potentials. In addition, electrochemical oxidation of the phosphinoselenoyl species displays an electrochemically irreversible oxidative wave, potentially due to the formation of a Se–Se bonded trication species. The $\%V_{bur}$ for the phosphinochalcogenyls decrease as the size of the chalcogen increases. The $\%V_{bur}$ for the cobaltocenium compounds is generally smaller than that of ferrocene analogues; however, there are potential complications with these calculations due to the asymmetry of the cobaltocenium compounds. The synthesis of several transition metal complexes bearing 1,1′-bis(phosphino)cobaltocenium ligands was also performed, with the solubility of such complexes depending substantially on the phosphine substituents. The X-ray structure of $[Au_2Cl_2(dppc)][PF_6]$ was determined and shows significant Au–Au interactions. The $\%V_{bur}$ for dppc is similar to that of dppf in analogous compounds. Electrochemistry of these complexes displayed at least two reductive waves, the first of which was reversible followed generally by at least one irreversible reductive wave. A correlation exists between the reduction potentials of cobaltocenium species and the potentials at which oxidation of analogous ferrocene species occur.

Acknowledgments

K.D.R., C.L.M., O.D.H. and C.N. thank the donors of the Petroleum Research Fund, administered by the American Chemical Society, for partial funding of this research, the Kresge Foundation for the purchase of the JEOL NMR, and the Academic Research Committee at Lafayette College for funding EXCEL scholars.

Appendix

CCDC No. 839626 for $[Au_2Cl_2(dppc)][PF_6]$, CCDC No. 839627 for [1-dtbpcS][PF_6], CCDC No. 839628 for [1-dtbpcSe][PF_6], CCDC No. 839629 for $[dcpcS_2][PF_6]$, CCDC No. 839630 for $[dcpcSe_2][PF_6]$, CCDC No. 839631 for $dcpfS_2$, CCDC No. 839632 for [dppc][PF_6], CCDC No. 839633 for $[dppcS_2][PF_6]$, CCDC No. 839634 for $[dppcSe_2][PF_6]$ and CCDC No. 840136 for $dcpfSe_2$; contains the supplementary crystallographic data for this paper. These data can be obtained free of charge from The Cambridge Crystallographic Data Centre via www.ccdc.cam.ac.uk/data_request/cif.

Appendix. Supplementary material

Supplementary material associated with this article can be found, in the online version, at doi:10.1016/j.jorganchem.2011.09.004

References

[1] D.L. DuBois, C.W. Eigenbrot Jr., A. Miedaner, J.C. Smart, R.C. Haltiwanger, Organometallics 5 (1986) 1405.

[2] K.S. Gan, T.S.A. Hor, in: A. Togni, T. Hayashi (Eds.), Ferrocenes: Homogeneous Catalysis, Organic Synthesis, Materials Science, VCH, New York, 1995 (Chapter 1).
[3] T. Hayashi, in: A. Togni, T. Hayashi (Eds.), Ferrocenes: Homogeneous Catalysis, Organic Synthesis, Materials Science, VCH, New York, 1995 (Chapter 2).
[4] S.W. Chien, T.S.A. Hor, in: P. Štěpnička (Ed.), Ferrocenes: Ligands, Materials and Biomolecules, John Wiley & Sons Ltd, West Sussex, England, 2008 (Chapter 2).
[5] T.J. Colacot, S. Parisel, in: P. Štěpnička (Ed.), Ferrocenes: Ligands, Materials and Biomolecules, John Wiley & Sons Ltd., West Sussex, England, 2008 (Chapter 3).
[6] P. Štěpnička, in: P. Štěpnička (Ed.), Ferrocenes: Ligands, Materials and Biomolecules, John Wiley & Sons Ltd., West Sussex, England, 2008 (Chapter 5).
[7] H.-U. Blaser, W. Chen, F. Camponovo, A. Togni, in: P. Štěpnička (Ed.), Ferrocenes: Ligands, Materials and Biomolecules, John Wiley & Sons Ltd., West Sussex, England, 2008 (Chapter 6).
[8] A.P. Shaw, J.R. Norton, D. Buccella, L.A. Sites, S.S. Kleinbach, D.A. Jarem, K.M. Bocage, C. Nataro, Organometallics 28 (2009) 3804.
[9] Y. Ren, G.-A. Yu, J. Guan, S.H. Liu, Appl. Organometal. Chem. 21 (2007) 1.
[10] T.J. Colacot, W.A. Carole, B.A. Neide, A. Harad, Organometallics 27 (2008) 5605.
[11] E.I. Rogers, D.S. Silvester, D.L. Poole, L. Aldous, C. Hardacre, R.G. Compton, J. Phys. Chem. C 112 (2008) 2729.
[12] P. Wasserscheid, T. Welton, Ionic Liquids In Synthesis. Wiley, Weinheim, Germany, 2002.
[13] J. Guan, G.-A. Yu, J.-G. Hou, N. Yu, Y. Ren, S.H. Liu, Appl. Organometal. Chem. 21 (2007) 355.
[14] C.C. Brasse, U. Englert, A. Salzer, H. Waffenschmidt, P. Wasserscheid, Organometallics 19 (2000) 3818.
[15] T. Fukuyama, M. Shinmen, S. Nishitani, M. Sato, I. Ryu, Org. Lett. 4 (2002) 1691.
[16] D.S. Shepard, B.F.G. Johnson, A. Harrison, S. Parsons, S.P. Smidt, L.J. Yellowlees, D. Reed, J. Organomet. Chem. 563 (1998) 113.
[17] I.M. Lorković, M.S. Wrighton, W.M. Davis, J. Am. Chem. Soc. 116 (1994) 6220.
[18] L.-C. Song, G.-A. Yu, F.-H. Su, Q.-M. Hu, Organometallics 23 (2004) 4192.
[19] A.B. Pangborn, M.A. Giardello, R.H. Grubbs, R.K. Rosen, F.J. Timmers, Organometallics 15 (1996) 1518.
[20] D.D. Perrin, W.L.F. Armarego, D.R. Perrin, Purification of Laboratory Chemicals, second ed. Pergamon, New York, 1985.
[21] G.-A. Yu, Y. Ren, J.-T. Guan, Y. Lin, S.H. Liu, J. Organomet. Chem. 692 (2007) 3914.
[22] Y. Chen, X.-H. Wu, G.-A. Yu, S. Jin, X.-G. Meng, S.-H. Liu, Transit. Met. Chem. 34 (2009) 103.
[23] J.-T. Guan, K.-C. Zhang, Z.-Q. Dai, Acta Crystallogr. Sect. E: Struct. Rep. Online 65 (2009) m960.
[24] G.M. Sheldrick, Acta Crystallogr. Sect. A 46 (1990) 467.
[25] G.M. Sheldrick, A.X.S. Bruker-, Software Reference Manuals. Bruker-AXS, Madison, WI, USA, 2001.
[26] A.L. Spek, J. Appl. Cryst. 36 (2003) 7.
[27] J.-G. Hou, P. Zhang, C. Ye, T.-G. Yu, Acta Crystallogr. Sect. E: Struct. Rep. Online 63 (2007) m2730.
[28] C. Hansch, A. Leo, R.W. Taft, Chem. Rev. 91 (1991) 165.
[29] N.G. Connelly, W.E. Geiger, Chem. Rev. 96 (1996) 877.
[30] C. Nataro, A.N. Campbell, M.A. Ferguson, C.D. Incarvito, A.L. Rheingold, J. Organomet. Chem. 673 (2003) 47.
[31] L.E. Hagopian, A.N. Campbell, J.A. Golen, A.L. Rheingold, C. Nataro, J. Organomet. Chem. 691 (2006) 4890.
[32] J.H.L. Ong, C. Nataro, J.A. Golen, A.L. Rheingold, Organometallics 22 (2003) 5027.
[33] F.N. Blanco, L.E. Hagopian, W.R. McNamara, J.A. Golen, A.L. Rheingold, C. Nataro, Organometallics 25 (2006) 4292.
[34] B.D. Swartz, C. Nataro, Organometallics 24 (2005) 2447.
[35] G. Pilloni, B. Corain, M. Degano, B. Longato, G. Zanotti, J. Chem. Soc. Dalton Trans. (1993) 1777.
[36] Z.-G. Fang, T.S.A. Hor, Y.-S. Wen, L.-K. Liu, T.C.W. Mak, Polyhedron 14 (1995) 2403.
[37] G. Pilloni, B. Longato, G. Bandoli, B. Corain, J. Chem. Soc. Dalton Trans. (1997) 819.
[38] $\%V_{bur}$ values were calculated using SambVca A. Poater, B. Cosenza, A. Correa, S. Giudice, F. Ragone, V. Scarano, L. Cavallo, Eur. J. Inorg. Chem. (2009) 1759.
[39] H. Clavier, S.P. Nolan, Chem. Commun. 46 (2010) 841.
[40] C.L. Mandell, S.S. Kleinbach, W.G. Dougherty, W.S. Kassel, C. Nataro, Inorg. Chem. 49 (2010) 9718.
[41] N. Meyer, F. Mohr, E.R.T. Tiekink, Acta Crystallogr. Sect. E: Struct. Rep. Online 66 (2010) m168.
[42] M. Necas, M. Beran, J.D. Woollins, J. Novosad, Polyhedron 20 (2001) 741.
[43] S. Lu, V.V. Strelets, M.F. Ryan, W.J. Pietro, A.B.P. Lever, Inorg. Chem. 35 (1996) 1013.
[44] O. Crespo, M.C. Gimeno, P.G. Jones, A. Laguna, Acta Crystallogr. Sect. C: Cryst. Struct. Commun. 56 (2000) 1433.
[45] E.C. Constable, C.E. Housecroft, M. Neuburger, S. Schaffner, E. Shardlow, Acta Crystallogr. Sect. E: Struct. Rep. Online 63 (2007) m1697.
[46] T.V. Segapelo, I.A. Guzei, J. Darkwa, J. Organomet. Chem. 693 (2008) 701.
[47] D.T. Hill, G.R. Girard, F.L. McCabe, R.K. Johnson, P.D. Stupik, J.H. Zhang, W.M. Reiff, D.S. Eggleston, Inorg. Chem. 28 (1989) 3529.
[48] F. Canales, M.C. Gimeno, P.G. Jones, A. Laguna, C. Sarroca, Inorg. Chem. 36 (1997) 5206.
[49] G. Bandoli, A. Dolmella, Coord. Chem. Rev. 209 (2000) 161.
[50] O.V. Gusev, A.M. Kalsin, M.G. Peterleitner, P.V. Petrovskii, K.A. Lyssenko, Organometallics 21 (2002) 3637.
[51] J.A. Davies, C.T. Eagle, D.E. Otis, U. Venkataraman, Organometallics 8 (1989) 1080.